Optical Fiber Technology 15 (2009) 258–265

Contents lists available at ScienceDirect

Optical Fiber Technology

www.elsevier.com/locate/yofte

Step-like all-optical decision function using nonlinear polarisation rotation in a Nonlinear Optical Loop Mirror and in a subsequent fibre section with output polarisation selection

O. Pottiez [a,*], B. Ibarra-Escamilla [b], E.A. Kuzin [b]

[a] Centro de Investigaciones en Óptica, Loma del Bosque 115, Col. Lomas del Campestre, 37150 León, Gto, Mexico
[b] Instituto Nacional de Astrofísica, Óptica y Electrónica (INAOE), Departamento de Óptica, L. E. Erro 1, Tonantzintla, 72000 Puebla, Pue., Mexico

ARTICLE INFO

Article history:
Received 13 August 2008
Revised 28 November 2008
Available online 23 December 2008

Keywords:
Sagnac interferometer
Fibre-optic devices
Optical signal processing

ABSTRACT

We propose and study numerically a fibre-based scheme designed to generate a step-like optical decision function for ultrafast data processing applications. The setup includes two main sections disposed in series: a Nonlinear Optical Loop Mirror with an output polariser on the one hand, and a circularly birefringent fibre span with a quarter wave retarder at the input and a polariser at the output on the other hand. Both sections operate through nonlinear polarisation rotation, and the switching characteristic is controlled through the light ellipticity, which can be adjusted by setting properly the orientation of the input polarisation, and by rotating the wave retarder and the two polarisers. For proper adjustment of these four parameters, a step-like optical decision function with ~10 dB/dB steepness is predicted. In the frame of all-optical regeneration, the setup allows eliminating ~76% peak-to-peak amplitude fluctuations on the marks and ~30% relative power on the spaces. We believe that this architecture should be considered for the design of ultrafast transmission networks and in the frame of all-optical computing applications.

1. Introduction

For many applications, like the regeneration of ultrafast data streams in future optical transmission networks, or the conception of logic decision functions and logic gates for ultrafast all-optical computing, the realisation of nearly step-like all-optical decision functions is a crucial issue. In the frame of all-optical regeneration, although 3R (reamplification, reshaping, retiming) techniques are required in some cases, the cheaper 2R (reamplification and reshaping only) solutions proved to be effective in most situations [1]. Ideal 2R regeneration is characterised by a step transfer function, which outputs a constant nonzero power level when the input signal power is above a given decision threshold, and zero power when the input power is below that threshold. Large amplitude fluctuations on the marks induced by noise, dispersion, nonlinearities, etc., in a transmission link are then eliminated, as well as the nonzero power level on the spaces, which originates in particular from the noise of optical amplifiers or ghost pulses. When regenerators are cascaded, the best regeneration performance is obtained for decision function shapes that are close to the ideal step function [2].

Very steep, nearly step-like transfer characteristics were obtained with semiconductor-based regenerators [2–4]. In the frame of ultrashort-pulsed on-off-keyed (OOK) signals at very high rates (40 Gb/s or beyond), however, this technology suffers from the intrinsically long carrier recovery time of semiconductor materials, which limits the operating speed of such devices. Devices based on ultrafast nonlinear effects in fibres, whose response time lies in the femtosecond range, are probably more promising for ultrahigh-speed regeneration, although a serious effort should be made to make these devices more compact, which now becomes possible through the use of high nonlinearity fibres [5,6]. One fibre-based technique relies on cascaded four-wave mixing [7–10], yielding near-ideal step-like transfer functions, although the setup is usually quite complicated, including one (or multiple) intense continuous-wave pump and a phase or frequency modulation scheme for both signal and pump in order to suppress stimulated Brillouin scattering. Another inconvenient of the technique is that the wavelength of the regenerated signal differs from the initial signal wavelength. Alternatively, a technique based on self-phase modulation in an optical fibre followed by offset filtering was demonstrated [11–17]. This technique also allows high-quality regeneration, and usually leads to simpler regenerator structures, as no pump source is needed. However it still imposes a wavelength change to the regenerated signal. Two stages are needed for

* Corresponding author.
E-mail address: pottiez@cio.mx (O. Pottiez).

1068-5200/$ – see front matter
doi:10.1016/j.yofte.2008.12.001

wavelength-shift-free regeneration, which complicates the setup [17].

Another all-fibre candidate is the nonlinear Sagnac interferometer, or Nonlinear Optical Loop Mirror (NOLM) [18]. Due to its simplicity and flexibility, this device is considered for many optical signal processing applications, including optical signal regeneration [1,19–30]. The NOLM is made of an optical coupler whose output ports are connected through a span of fibre. In conventional designs, a power asymmetry is generated, usually through the use of an asymmetric coupling ratio [18,21,24], or by introducing attenuation [19,20,22] or gain [31] asymmetrically in the loop. Alternatively, power asymmetry is due to asymmetric pulse stretching in dispersion-imbalanced schemes [23,32,33]. In most power-imbalanced schemes, the nonlinear transfer (or switching) characteristic is due to the Self-Phase Modulation (SPM) optical Kerr effect, which ensures that a nonlinear phase shift difference appears between the counter-propagating beams. It is well known that, in standard fibre, the residual birefringence causes changes in the polarisation of each beam during propagation. This polarisation evolution in the loop is not controlled, however, and the polarisation state varies randomly, tending to take all possible values through the fibre. As a consequence, the nonlinear polarisation rotation (NPR) tends to average out over the fibre. The device typically exhibits a sinusoidal transmission characteristic. If the NOLM is properly biased (usually through a polarisation controller inside the loop), this switching characteristic presents a minimum at zero input power and a maximum for some nonzero value of power, called the switching power. In the frame of regeneration, low transmission at low power allows the elimination of residual optical power on spaces, whereas amplitude fluctuations on the marks can be eliminated if their average power is adjusted slightly beyond maximal transmission, where the input–output power characteristic of the NOLM presents a maximum. One drawback of the NOLM however is that the sinusoidal function is intrinsically far from the ideal step function. In particular, the minimum and maximum of the input–output power characteristic are not very extended, and the curve steepness is low. This limits the level of background noise on the spaces and the amplitude of fluctuations on the marks that can be suppressed using this setup. If a strongly power-imbalanced coupler ($\sim$0.9/0.1) is used, a plateau appears in the input–output power characteristic, so that large amplitude fluctuations on the marks can be suppressed. In this case however, the spaces are not efficiently regenerated, as low-power transmission is large [21].

An alternative NOLM design was proposed, which exploits polarisation asymmetry for switching instead of power imbalance [34]. It includes a 50/50 coupler, low-birefringence, highly twisted fibre, and a quarter-wave retarder (QWR) as the symmetry-breaking element. As the scheme is power-symmetric, SPM plays no significant role in the device operation, and switching is due to NPR. Due to the presence of the QWR, which is inserted after one of the coupler output ports, the two beams propagate in the loop with different polarisation states, ensuring a NPR difference that is responsible for switching. High twist generates optical activity in the fibre and provides a nearly ideal isotropic medium [35], which prevents the polarisation states from averaging out during propagation, and allows NPR to accumulate. This polarisation-controlled scheme yields more flexibility of the switching characteristic than conventional SPM-based schemes. For example, for a particular adjustment of the QWR angle, a sinusoidal switching characteristic is obtained with zero minimal transmission at low power. For another QWR angle, a characteristic very similar to that of the strongly power-imbalanced scheme [21], adapted for reducing large amplitude fluctuations on marks, is obtained [36]. However, although even non-sinusoidal transmission characteristics can be obtained with this scheme, these still strongly depart from a step-like function.

A noticeable step forward was realised when the NPR-based scheme described above was considered together with a polariser inserted after the NOLM output [37]. By controlling the input polarisation state as well as the polariser orientation, the maximum of the NOLM input–output power characteristic was converted into a very wide plateau, allowing the elimination of large amplitude fluctuations on marks. The low-power portion of the characteristic, however, and the curve steepness, were still similar to those of a sine function. For other adjustments, a wide low-transmission region was obtained at low power, at the price however of a high switching power and a narrowing of the maximum. For still other adjustments of the parameters, a substantial enhancement of the steepness of the transfer function was obtained [38]. In none of these cases, however, a step-like function was obtained.

Finally, a simple method to obtain a power-dependent transmission characteristic consists in using a section of fibre in which light undergoes NPR, followed by a polariser which converts the polarisation rotation into an amplitude modulation. This principle was used to realise artificial saturable absorbers for mode-locked fibre lasers. In the frame of optical signal shaping applications, such a design allowed 10-fold temporal narrowing of optical pulses [39]. However, the transfer function still appeared to be nearly sinusoidal at moderate power and such a large shortening factor required the pulse peak power to be increased to several times the first transmission maximum. As a consequence, a substantial pedestal was accompanying the narrowed pulses.

In this paper, we propose to extend the above NPR-based NOLM with output polariser setup using an additional fibre span in which light undergoes NPR, followed by a polariser. For proper adjustment of the parameters, we show that a nearly truly step-like switching characteristic is obtained.

2. Modelling

The proposed setup is shown in Fig. 1. The power-symmetric NOLM is made of a 50/50 coupler, a length L_N of low-birefringence twisted fibre and a QWR (QWRN) inserted after one of the coupler output ports. At the NOLM output, a polariser P1 selects a particular linear polarisation component of the output beam. Linear polarisation is then turned to elliptic through a QWR (QWR1). The light then propagates through a section of low-birefringence, highly twisted fibre with length L_R, in which polarisation rotation takes place. Finally, at the fibre output, light goes through a second polariser P2. The input polarisation to the NOLM is chosen linear (first Stokes parameter at NOLM input $A_{c,in} = 0$), and the QWRN angle is adjusted to the value ensuring zero low-power NOLM transmission, which we use as reference. The angles χ_1 of P1, α_1 of QWR1, χ_2 of P2 and ψ_{in} of the input polarisation are all taken with respect to the QWRN axis.

The present analysis uses a continuous-wave approach, so that chromatic dispersion is neglected. In the case of ultrashort-pulsed ($\sim$1-ps) signals, this approach still constitutes a valid approximation if high nonlinearity fibres are used, due to the short fibre lengths involved (down to a few meters) and the possibility to design at will the dispersion characteristic of photonic crystal fibres [5,6]. The NOLM section of the setup presented in Fig. 1 was studied previously for linear input polarisation [40]. In the weak nonlinearity limit [34], and for high twist, its power transmission is given by

$$T_N = \frac{P_{NP1}}{P_{in}} = \frac{1}{2} - \frac{1}{2}\cos(\pi P_{in}/P_{\pi\psi}), \tag{1}$$

where P_{in} and P_{NP1} are the NOLM input and output powers, respectively, and $P_{\pi\psi} = 4\pi/[\beta_N L_N|\sin(2\psi_{in})|]$ is the switching

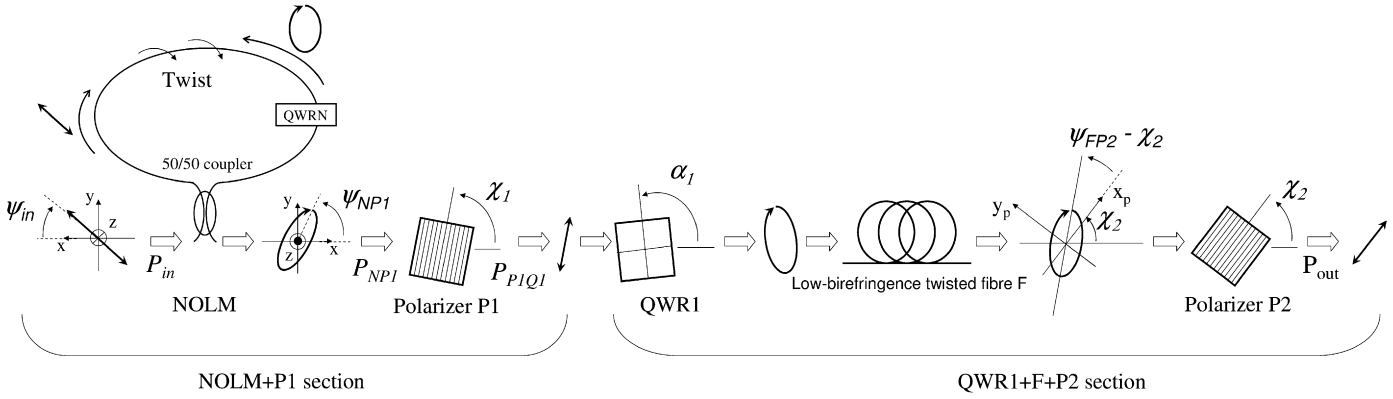

Fig. 1. Configuration under study.

power, where β_N is the fibre nonlinear coefficient for circular polarisation [34], and L_N is the loop length. It appears that $P_{\pi\psi}$ depends on the input polarisation orientation, ψ_{in}. Its minimal value $P_{\pi N} = 4\pi/\beta_N L_N$ is obtained for $\psi_{in} = \pi/4$, when the polarisation asymmetry of the counter-propagating beams is maximal (one beam is linear and the other one is circular), whereas its maximum tends to infinity for $\psi_{in} = 0$, when both polarisations are linear, and no polarisation asymmetry occurs. The input polarisation orientation thus allows adjusting the switching power between a finite minimal value and infinity. At the NOLM output, the Stokes parameter $|A_{c,NP1}| = \sin(2\psi_{in})$ also depends on ψ_{in}, but is independent of input power. Hence the ellipticity at the NOLM output is not modified as input power is increased, although the ellipse rotates proportionally to power, with its orientation given by $\psi_{NP1} = \pi P_{in}/2P_{\pi\psi}(+\pi/2)$. From these relations, the transmission of the NOLM output beam through the polariser P1 can be easily calculated, and writes as [37]:

$$T_{P1} = \frac{P_{P1Q1}}{P_{NP1}} = \frac{1}{2} - \frac{1}{2}\cos(2\psi_{in})\cos(\pi P_{in}/P_{\pi\psi} - 2\chi_1). \tag{2}$$

Note that, although T_{P1} is defined as the ratio between the power at the P1 output and the power at the NOLM output, it is given in Eq. (2) as a function of power at the NOLM input, P_{in}. It appears from Eq. (2) that the amplitude of T_{P1} is determined by the polarisation orientation ψ_{in} at the NOLM input, and its phase through the P1 orientation, χ_1. By adjusting these two parameters adequately, T_{P1} can be employed to smoothen the peak of T_N [see Fig. 2(a)]. This makes it possible to obtain a flat plateau in the output power characteristic of the NOLM + P1, $P_{P1Q1} = T_{NP1} \times P_{in} = T_N T_{P1} \times P_{in}$ [see Fig. 2(b)]. Note also that the periodicity of T_{P1}, determined by $P_{\pi\psi}$, is the same as for T_N.

At the P1 output, the linearly polarised light can be represented by the following Jones vector in the $[C^+, C^-]$ basis of circular polarisation:

$$E_{P1Q1} = \sqrt{\frac{P_{P1Q1}}{2}}\begin{bmatrix} e^{i\chi_1} \\ e^{-i\chi_1} \end{bmatrix}. \tag{3}$$

The beam then goes through the QWR1, which is tilted by an angle α_1. In the $[C^+, C^-]$ basis, the QWR1 can be described by the matrix [41]

$$QWR1 = \begin{bmatrix} \frac{1+i}{2} & \frac{1-i}{2}e^{2i\alpha_1} \\ \frac{1-i}{2}e^{-2i\alpha_1} & \frac{1+i}{2} \end{bmatrix}. \tag{4}$$

The field at the QWR1 output is then given by

$$\begin{aligned} E_{Q1F} &= QWR1 \times E_{P1Q1} \\ &= \sqrt{P_{P1Q1}}\begin{bmatrix} \cos(\chi_1 - \alpha_1 + \pi/4)e^{i\alpha_1} \\ \sin(\chi_1 - \alpha_1 + \pi/4)e^{-i\alpha_1} \end{bmatrix}. \end{aligned} \tag{5}$$

Eq. (5) shows that the ellipticity of the light polarisation depends on the relative orientation $\chi_1 - \alpha_1$ between QWR1 and P1. The orientation of QWR1 is used to adjust the light ellipticity at the fibre input. The Stokes parameter at this point can be easily calculated by

$$A_{c,Q1F} = \frac{|C^+|^2 - |C^-|^2}{|C^+|^2 + |C^-|^2} = \sin\big[2(\alpha_1 - \chi_1)\big]. \tag{6}$$

After the QWR1, light propagates through a length L_R of circularly birefringent fibre. Polarisation evolution can be described by the nonlinear equations in the continuous-wave case [42], which write as

$$\begin{aligned} dC^+/dz &= i\rho C^+ + i\beta_R P_{P1Q1}\left(\frac{3}{2} - \frac{1}{2}A_{c,Q1F}\right)C^+; \\ dC^-/dz &= -i\rho C^+ + i\beta_R P_{P1Q1}\left(\frac{3}{2} + \frac{1}{2}A_{c,Q1F}\right)C^-. \end{aligned} \tag{7}$$

In Eq. (7), ρ is the rotatory power ($\sim$5% of the twist rate), β_R is the nonlinearity coefficient and d/dz denotes the first derivative with respect to the direction of propagation z. In the weak nonlinearity approximation [34], the Stokes parameter does not vary along z, so that Eq. (7) can be integrated easily, and a Jones matrix representation of the fibre can be obtained as

$$F = \begin{bmatrix} e^{i[\rho + \beta_R P_{P!Q1}(\frac{3}{2} - \frac{1}{2}A_{c,Q1F})]L_R} & 0 \\ 0 & e^{i[-\rho + \beta_R P_{P1Q1}(\frac{3}{2} + \frac{1}{2}A_{c,Q1F})]L_R} \end{bmatrix}. \tag{8}$$

This matrix includes both linear and nonlinear polarisation rotation effects, as well as a nonlinear phase shift. At the fibre output, the Jones vector is given by

$$\begin{aligned} E_{FP2} &= FE_{Q1F} \\ &= \sqrt{P_{P1Q1}}\begin{bmatrix} \cos(\chi_1 - \alpha_1 + \pi/4)e^{i(\alpha_1 + \rho L_R - \frac{1}{2}A_{c,Q1F}\beta_R P_{P1Q1}L_R)} \\ \sin(\chi_1 - \alpha_1 + \pi/4)e^{-i(\alpha_1 + \rho L_R - \frac{1}{2}A_{c,Q1F}\beta_R P_{P1Q1}L_R)} \end{bmatrix} \\ &\quad \times e^{i\frac{3}{2}\beta_R P_{P1Q1}L_R} \\ &= \sqrt{P_{P1Q1}}\begin{bmatrix} \cos(\chi_1 - \alpha_1 + \pi/4)e^{i\psi_{FP2}} \\ \sin(\chi_1 - \alpha_1 + \pi/4)e^{-i\psi_{FP2}} \end{bmatrix}e^{i\varphi}. \end{aligned} \tag{9}$$

One can verify easily from Eq. (9) that the Stokes parameter (and thus the ellipticity) at the fibre output is not modified from the fibre input [Eqs. (5) and (6)], and only the output ellipse orientation $\psi_{FP2} = \alpha_1 + \rho L_R - 1/2A_{c,Q1F}\beta_R P_{P1Q1}L_R$ is modified and depends on power, due to nonlinear polarisation rotation. At this stage it is convenient to define a new reference system $[x_p, y_p]$ associated with the polariser P2 (x_p parallel to the direction of polariser

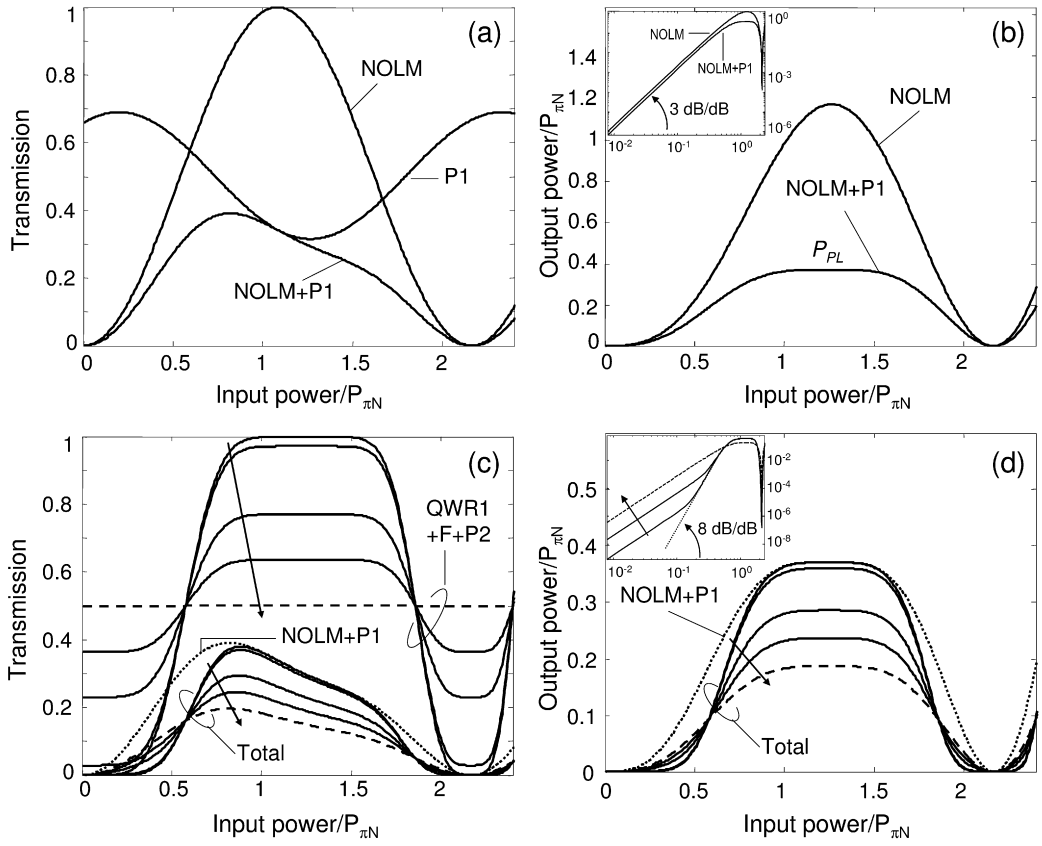

Fig. 2. (a) Transmission of NOLM, P1 and NOLM + P1 for $\psi_{in} = 0.75\pi/4$ and $\chi_1 = -0.19$; (b) Corresponding output power characteristic of NOLM and NOLM + P1; powers are normalised to the minimal NOLM switching power $P_{\pi N}$. Inset: curves in logarithmic scale; (c) Transmission of QWR1 + F + P2 and total transmission of the setup; and (d) Corresponding total output power characteristics; several examples were calculated for values of $L_R = 10$, 2, 0.8, 0.7 and 0.673, in units of $L_N\beta_N/\beta_R$ (in the sense of the arrows), and respective values of $\alpha_1 - \chi_1 = -0.034$, -0.17, -0.50, -0.65 and $-\pi/4$, ensuring $P_{\pi/2} = P_{PL}$ in each case. Inset: curves shown in logarithmic scale for $L_R = 10$, 2 and $0.673 \times L_N\beta_N/\beta_R$. NOLM + P1 transmission and output power characteristics were reproduced in (c) and (d) for comparison (dotted lines).

transmission, see Fig. 1). The corresponding basis of circular polarisation is $[C_p^+, C_p^-]$ with $C_p^+ = C^+\exp(i\chi_2)$ and $C_p^- = C^-\exp(-i\chi_2)$, and related to $[x_p, y_p]$ through

$$\begin{bmatrix} x_p \\ y_p \end{bmatrix} = \begin{bmatrix} \sqrt{2}/2 & \sqrt{2}/2 \\ -i\sqrt{2}/2 & i\sqrt{2}/2 \end{bmatrix} \begin{bmatrix} C_p^+ \\ C_p^- \end{bmatrix}. \tag{10}$$

In this circular basis, Eq. (9) becomes

$$E'_{FP2} = \sqrt{P_{P1Q1}} \begin{bmatrix} \cos(\chi_1 - \alpha_1 + \pi/4)e^{i(\psi_{FP2} - \chi_2)} \\ \sin(\chi_1 - \alpha_1 + \pi/4)e^{-i(\psi_{FP2} - \chi_2)} \end{bmatrix} e^{i\varphi}. \tag{11}$$

The polariser P2 will select the x_p component of the field, so that using Eqs. (10) and (11) one can determine the expression of the power transmission for the QWR1 + F + P2 segment. After some algebra, it writes as

$$T_R = \frac{P_{out}}{P_{P1Q1}} = \frac{|x_p|^2}{P_{P1Q1}} = \frac{|C_p^+ + C_p^-|^2}{2P_{P1Q1}} = \frac{1}{2}\left[1 + \cos 2(\alpha_1 - \chi_1)\cos 2(\psi_{FP2} - \chi_2)\right]. \tag{12}$$

In Eq. (12), ψ_{FP2} is a function of power, which can be conveniently rewritten as

$$\psi_{FP2} = \psi_0 - \frac{\pi}{2}\frac{P_{P1Q1}}{P_{\pi/2}},$$

$$\text{with} \quad \psi_0 = \alpha_1 + \rho L_R \quad \text{and} \quad P_{\pi/2} = \frac{\pi}{\beta_R L_R \sin 2(\alpha_1 - \chi_1)}, \tag{13}$$

where $P_{\pi/2}$ is the power difference between a minimum and a maximum of T_R, corresponding to a $\pi/2$ nonlinear ellipse rotation. Eqs. (12) and (13) show that T_R is a sinusoidal function of P_{P1Q1}, whose dynamic range $\cos 2(\alpha_1 - \chi_1)$ and periodicity $2P_{\pi/2}$ are determined by $\alpha_1 - \chi_1$, the relative angle between the QWR1 and P1, and whose phase is $\psi_0 - \chi_2$. Hence the QWR1 angle allows adjusting the dynamic range and periodicity of T_R, whereas its phase can be adjusted through the P2 orientation.

Using Eqs. (1)–(2) and (12)–(13), one can now determine the global transmission of the setup presented in Fig. 1, which writes as

$$T = T_{NP1}(P_{in}) \times T_R(P_{P1Q1}) = T_{NP1}(P_{in}) \times T_R\left[T_{NP1}(P_{in})P_{in}\right]. \tag{14}$$

It should be noted in Eq. (14) that the transmission of the NOLM + P1, T_{NP1}, does not only multiply T_R, but also appears in the argument of T_R.

3. Analysis and discussion

As it was shown in [37] [see also Eq. (2)], by adjusting the amplitude of T_{P1} through the polarisation orientation ψ_{in} at the NOLM input, and its phase through the P1 angle χ_1, one can manage to generate a flat top in the transmitted power characteristic of the NOLM + P1 combination. At this point, the first three derivatives of the output power characteristic cancel out simultaneously (3rd-order maximum). Fig. 2(a) shows the transmission functions T_N of the NOLM, T_{P1} of polariser P1 and $T_{NP1} = T_N T_{P1}$ of the NOLM + P1, and Fig. 2(b) presents the corresponding output power characteristics of the NOLM and of the NOLM + P1 when the parameters ψ_{in} and χ_1 are properly adjusted. An extended flat top is observed in the NOLM + P1 output power characteristic. The value of input power at the plateau centre is only 1.25 times higher than the minimal NOLM switching power, $P_{\pi N} = 4\pi/\beta_N L_N$, which is

obtained when the input polarisation makes an angle of 45° with the QWRN axes ($\psi_{in} = \pi/4$). The transmission T_{NP1} at this point is ~3 times lower than the transmission T_N of the NOLM alone. Assuming that the average mark level at the NOLM input is adjusted to the plateau centre, peak-to-peak amplitude fluctuations as large as 33% can be reduced to within 1% using the NOLM + P1 setup. This flat top characteristic is responsible for the excellent signal-to-noise ratio (SNR) improvement properties of the setup [37]. In comparison, if the NOLM alone is used, its 1st-order maximum allows input fluctuations not higher than ~10% to be reduced to 1%. In contrast, in terms of extinction ratio (ER, defined as the power ratio between marks and spaces), no improvement is obtained when the NOLM + P1 is used instead of the NOLM alone. Actually, the ER at the NOLM output is even slightly degraded after P1 [37]. If the average mark power at the NOLM input matches the maximum of the output power curve, a relative input power on the spaces (1/ER) of 14% using the NOLM alone and of 11% with the NOLM + P1 can be reduced to 1%. This can be explained by observing that the output power characteristics of both NOLM and NOLM + P1 are similar near zero input power, where a 2nd-order minimum is obtained in each case [Fig. 2(b)]. The ER degradation after P1 results from the ~3-fold reduction of the maximum output power (mark power). Finally, both transitions present a maximal slope of ~3 dB/dB, a value compatible with the cubic growth of the output power characteristics at low input power [inset in Fig. 2(b)].

For the same adjustments of ψ_{in} and χ_1, we calculated the transmission of the QWR1 + F + P2 segment, $T_R(T_{NP1} \times P_{in})$. Parameters were chosen in order to ensure minimal T_R at zero input power and maximal T_R for the $T_{NP1} \times P_{in}$ value at the plateau maximum in Fig. 2(b), $P_{PL} \approx 0.371 P_{\pi N}$. Looking at Eqs. (12) and (13), the first condition implies that $\chi_2 = \psi_0 + \pi/2$, which imposes the P2 orientation χ_2, and the second condition means that $P_{\pi/2} = P_{PL}$. The value of $P_{\pi/2}$ is thus imposed. Assuming a given nonlinear coefficient β_R in Eq. (13), either the fibre length L_R or the QWR1 angle α_1 can still be chosen, which leaves one degree of freedom. A given value of $P_{\pi/2}$ can be obtained using in Eq. (13) a large value for L_R together with an angle α_1 close to χ_1, or a short L_R with an angle α_1 that substantially deviates from χ_1. The latter solution however leads to a degradation of the T_R dynamic range, as shown in Eq. (12). This can be explained by considering that the NPR effect is stronger when the light ellipticity, or equivalently the modules of the first Stokes parameter is higher. If the fibre length is large, for $P_{\pi/2}$ input power a small value of ellipticity [associated with a small value of $\alpha_1 - \chi_1$, see Eq. (6)] yielding slow NPR will still allow to accumulate a $\pi/2$ nonlinear ellipse rotation to the fibre output. Hence the transmission through P2 will increase from a minimum to a maximum when the power is increased from 0 (ellipse minor axis aligned with P2) to $P_{\pi/2}$ (major axis aligned with P2). If the polarisation is close to linear, minimal and maximal transmission values through P2 are close to 0 and 1, respectively. If now the fibre is short, a larger ellipticity yielding faster NPR will be required to get a $\pi/2$ nonlinear rotation over the reduced fibre span. A large ellipticity is associated with reduced variations of transmission through P2 as the ellipse rotates at the polariser input. Fig. 2(c) shows the T_R characteristic of the QWR1 + F + P2 segment for several pairs of L_R and $\alpha_1 - \chi_1$ values that ensure a $\pi/2$ nonlinear ellipse rotation over the fibre. The corresponding total transmission T is also shown in each case. Fig. 2(d) presents the corresponding output power characteristics.

Fig. 2(d) shows that, for large values of L_R, the output power characteristic presents a flat plateau at high power, an extended region at low power over which the output power remains close to zero, and a sharp transition between these two regions. By analysing Eq. (14), it appears that the plateau is a 3rd-order maximum (where the first three derivatives of output power cancel out). Besides, considering that $T_R(0) = 0$, the output power characteristic would present an eighth-order minimum at $P_{in} = 0$, and grow as the ninth power of P_{in}. Although in practise $T_R(0) \neq 0$ as the minor axis of the polarisation ellipse is transmitted through P2 at low power, for the largest value of L_R considered, a maximal slope of 8 dB/dB is still observed (Fig. 2(d), inset). In comparison with the NOLM + P1, the 3rd-order plateau is thus maintained in the proposed configuration, whereas the flatness at low power is considerably increased. Considering again that the power on the spaces at the device output should be kept within 1% of the average power on marks, a space-to-mark power ratio as high as 29% is acceptable at the device input [curve $L_R = 10 L_N \beta_N / \beta_R$ in Fig. 2(d)]. In comparison with the NOLM + P1 scheme, the proposed setup allows to regenerate spaces carrying more than 2.5 times higher optical power. For small values of L_R however, the curve sharpness and the extension of the low-power region diminish. A limit case is found when the fibre is so short that circular polarisation (corresponding to fastest NPR) is required. In this case, $\alpha_1 - \chi_1 = \pi/4$, and considering the relations $P_{\pi/2} = P_{PL} \approx 0.371 P_{\pi N}$, $P_{\pi N} = 4\pi/\beta_N L_N$ as well as Eq. (13), it comes that $L_R \approx 0.673 L_N \beta_N / \beta_R$, which is the minimal fibre length allowing a $\pi/2$ nonlinear ellipse rotation. For circular polarisation however, transmission through P2 is independent of the ellipse orientation, and thus of power (see Fig. 2(c), dashed). The total transmission is thus identical to that of the NOLM + P1 setup, except for the 3-dB loss through P2 (Fig. 2(d), dashed).

The above discussion shows that it is important to ensure that L_R is large enough in order to take advantage of the second section of the proposed setup. Although theoretically the optimal situation is obtained for $L_R = \infty$, the value of L_R can be kept reasonably small in practise. As an example, Fig. 2 (c and d) shows that the curves obtained for $L_R = 10 L_N \beta_N / \beta_R$ and $2 L_N \beta_N / \beta_R$ are very close to each other. The width of the low-power region in the latter case is not substantially reduced with respect to the former case, although the fibre length employed is five times smaller. As to amplitude noise reduction, the performances of the proposed setup are comparable with those of the NOLM + P1 for all values of L_R. For $L_R = 10 L_N \beta_N / \beta_R$ and $2 L_N \beta_N / \beta_R$, fluctuations as large as 32.5% can be reduced to within 1%.

Let us also stress the importance of using low-birefringence fibre in the second section of the setup for the proposed application. Indeed, in configurations based on highly birefringent fibre, the group velocity mismatch between orthogonal polarisation modes causes a temporal shift between the polarisation components of ultrashort pulses. Although this effect can be useful for realising optical derivators [43], it would be detrimental for the present application. Finally, in highly birefringent fibre, phase matching can enhance the conversion of the signal into Stokes and anti-Stokes components at new frequencies in the orthogonal polarisation mode, through four-wave mixing [44].

The power transfer function of the setup depicted in Fig. 1 can be made even closer to the ideal step function if the adjustment parameters are slightly modified from those of Fig. 2. First, ψ_{in} (and to a lesser extent χ_1) is modified in order to increase slightly the amplitude of T_{P1}, which has the effect of widening the plateau of the NOLM + P1 output power characteristic, T_{NP1}, at the price of some ripple appearing on the plateau [Fig. 3(b)]. On the other hand, α_1 and χ_2 are adjusted in such a way that $P_{\pi/2}$ is made slightly smaller than the maximal value P_{PL} of $T_{NP1} \times P_{in}$, and that the QWR1 + F + P2 transmission T_R reaches its minimum for a nonzero value of input power, and its maximum for a value of $T_{NP1} \times P_{in}$ slightly below P_{PL} [Fig. 3(a)]. As a result for the total output power characteristic $T P_{in}$, the width of the low-power region and particularly of the plateau are substantially increased, at the price of some ripple and a small increase of

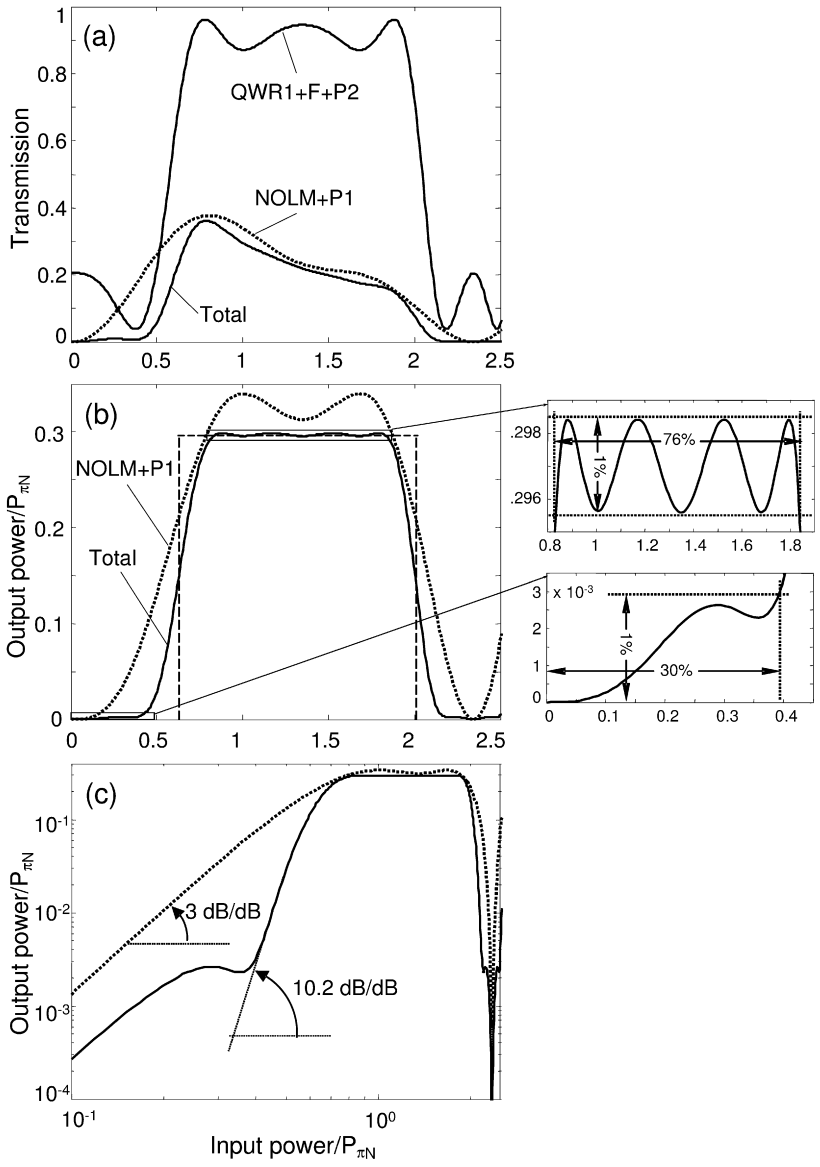

Fig. 3. (a) Transmission of the NOLM + P1, QWR1 + F + P2 and total transmission of the setup for $\psi_{in} = 0.65\pi/4$, $\chi_1 = -0.20$, $\alpha_1 = \chi_1 + 0.25\pi/4$, $\chi_2 = \psi_0 + 0.72\pi/2$ and $L_R = 2.8 \times L_N\beta_N/\beta_R$; (b) Corresponding NOLM + P1 and total output power characteristics, with insets showing details of the plateau and low-power regions; thin dashed line shows an ideal step transfer function for comparison; (c) Curves of (b) shown in logarithmic scale.

the input power at the plateau centre. The steepness of the transition between these two regions is also significantly improved. The curves of Fig. 3 were obtained when the above mentioned parameters were optimised in order to maximise the widths of the high-power plateau and low-power region, assuming that the residual output amplitude fluctuation on the marks and relative power on the spaces should be kept within 1% at the device output, when the input average mark power is adjusted to the plateau centre. The widths of the plateau and low-power region relative to the plateau centre are found to be ∼76% and ∼30%, respectively. As a comparison, for the ideal step function shown in Fig. 3(b) (thin dashed), these values are 100% and 50%, respectively. The plateau width is thus increased by a factor higher than two with respect to the case of Fig. 2. The maximal steepness is slightly above 10 dB/dB [Fig. 3(c)]. In this region, an output power increase of 9.6 dB (16.8 dB) is obtained for an input power increase of 1 dB (2 dB). Such values surpass by far those obtained with other NOLM-based setups and support the comparison with other nonlinear fibre-based switches [7–17] or with semiconductor-based setups [4].

Although the continuous-wave analysis presented here remains valid for ultrashort-pulsed signals if high nonlinearity fibres with properly designed dispersion are used in the setup, an important issue is related to the substantial reshaping undergone by the pulses through such a regenerator. Fig. 4 (solid curves) illustrates this reshaping for the regenerator adjustments corresponding to Fig. 3, in the case of Gaussian input pulses. It appears in particular that, for input peak power values corresponding to the upper end of the plateau in the transfer characteristic, the emerging pulses are nearly rectangular. Such reshaping may be detrimental in the case of in-line regenerators, as further propagation of the pulses in dispersive and nonlinear fibre will lead to further alteration of the pulse profile, with possibly the formation of background radiation. As a consequence, if further propagation is planned after the regenerator, the fibre parameters should be chosen in order to minimise pulse profile deformation. In particular, the fibre dispersion at the signal wavelength and its nonlinear coefficient should be small. Fig. 4 also offers an additional illustration of the capabilities of the device for the regeneration of the mark level, and for the elimination of ghost pulses (dashed curves).

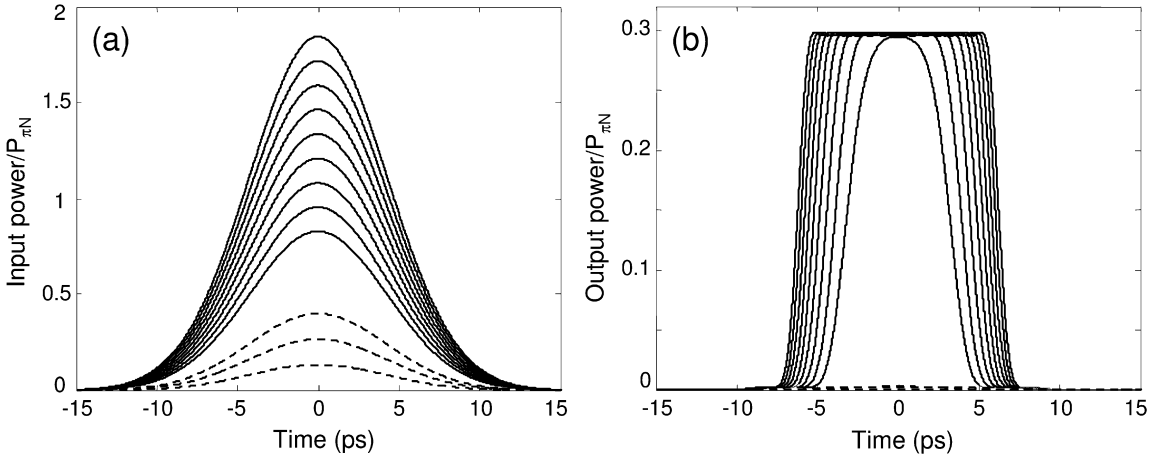

Fig. 4. (a) Intensity profiles of input Gaussian pulses with 10-ps full-width at half maximum duration and different amplitudes; (b) Corresponding profiles at the device output when parameters of Fig. 3 are used.

4. Conclusion

In this paper we propose and analyse numerically a novel fibre-based architecture to produce a step-like optical decision function. The device is composed of two sections. The first section is a NPR-based NOLM with output polarisation selection and the second one is a circularly birefringent fibre span with input QWR and output polariser, where NPR takes place. Both input and output polarisation states are linear. When the input polarisation angle together with the orientations of the QWR and of the two polarisers are properly adjusted, a step-like switching characteristic is obtained, which presents a maximal transmission as high as about 30% of the NOLM maximal transmission. The first section is responsible for the appearance of a wide plateau at a power slightly beyond the NOLM switching power, whereas the second section generates an extended region at low power where output power cancels out, and also extends considerably the high-power plateau. Proper operation of the second section requires however a sufficient length of circularly birefringent fibre. For comparable values of the fibre nonlinear coefficients, a fibre length two to three times larger than the NOLM length is a reasonable choice for the second section. In the frame of all-optical regeneration, imposing residual amplitude fluctuations on the marks and residual space-to-mark power ratio within 1%, amplitude fluctuations on the marks as large as ∼76% and spaces carrying optical powers as high as ∼30% of the mark level can be regenerated using the proposed scheme. Switching steepness as high as 10 dB is obtained. Taking advantage of the new developments in high-nonlinearity fibres, this work could lead to the development of compact all-fibre optical gates to be used in future ultrafast photonic networks and optical computing.

Acknowledgments

O. Pottiez was supported by CONACyT grant 53990.

References

[1] S. Boscolo, S.K. Turitsyn, V.K. Mezentsev, Performance comparison of 2R and 3R optical regeneration schemes at 40 Gb/s for application to all-optical networks, J. Lightwave Technol. 23 (2005) 304–309.
[2] O. Leclerc, B. Lavigne, E. Balmefrezol, P. Brindel, L. Pierre, D. Rouvillain, F. Seguineau, Optical regeneration at 40 Gb/s and beyond, J. Lightwave Technol. 21 (2003) 2779–2790.
[3] K. Nonaka, Y. Noguchi, H. Tsuda, T. Kurokawa, Digital signal regeneration with side-injection-light-controlled bistable laser diode as a wavelength converter, IEEE Photon. Technol. Lett. 7 (1995) 29–31.
[4] W. D'Oosterlinck, G. Morthier, M.K. Smit, R. Baets, Very steep optical thresholding characteristic using a DFB laser diode and an SOA in an optical feedback scheme, IEEE Photon. Technol. Lett. 17 (2005) 642–644.
[5] http://www.crystal-fibre.com/products/nonlinear.shtm.
[6] H. Ebendorff-Heidepriem, P. Petropoulos, S. Asimakis, V. Finazzi, R.C. Moore, K. Frampton, F. Koizumi, D.J. Richardson, T.M. Monro, Bismuth glass holey fibers with high nonlinearity, Opt. Express 12 (2004) 5082–5087.
[7] S. Yamashita, M. Shahed, Optical 2R regeneration using cascaded fiber four-wave mixing with suppressed spectral spread, IEEE Photon. Technol. Lett. 18 (2006) 1064–1066.
[8] E. Ciaramella, F. Curti, S. Trillo, All-optical signal reshaping by means of four-wave mixing in optical fibers, IEEE Photon. Technol. Lett. 13 (2001) 142–144.
[9] S. Radic, C.J. McKinstrie, R.M. Jopson, J.C. Centanni, A.R. Chraplyvy, All-optical regeneration in one- and two-pump parametric amplifiers using highly nonlinear optical fiber, IEEE Photon. Technol. Lett. 15 (2003) 957–959.
[10] A. Bogris, D. Syvridis, Regenerative properties of a pump-modulated four-wave mixing scheme in dispersion-shifted fibers, J. Lightwave Technol. 21 (2003) 1892–1902.
[11] P.V. Mamyshev, All-optical data regeneration based on self-phase modulation effect, in: Proc. European Conference on Optical Communications, Madrid, Spain, 1998, pp. 475–476.
[12] T.-H. Her, G. Raybon, C. Headley, Optimization of pulse regeneration at 40 Gb/s based on spectral filtering of self-phase modulation in fiber, IEEE Photon. Technol. Lett. 16 (2004) 200–202.
[13] M. Matsumoto, Performance analysis and comparison of optical 3R regenerators utilizing self-phase modulation in fibers, J. Lightwave Technol. 22 (2004) 1472–1482.
[14] L. Provost, C. Finot, P. Petropoulos, K. Mukasa, D.J. Richardson, Design scaling rules for 2R-optical self-phase modulation-based regenerators, Opt. Express 15 (2007) 5100–5113.
[15] A.G. Striegler, B. Schmauss, Analysis and optimization of SPM-based 2R signal regeneration at 40 Gb/s, J. Lightwave Technol. 24 (2006) 2835–2843.
[16] M. Rochette, J.L. Blows, B.J. Eggleton, 3R optical regeneration: An all-optical solution with BER improvement, Opt. Express 14 (2006) 6414–6427.
[17] M. Matsumoto, Efficient all-optical 2R regeneration using self-phase modulation in bidirectional fiber configuration, Opt. Express 14 (2006) 11018–11023.
[18] N.J. Doran, D. Wood, Nonlinear-optical loop mirror, Opt. Lett. 13 (1988) 56–58.
[19] M.D. Pelusi, Y. Matsui, A. Suzuki, Pedestal suppression from compressed femtosecond pulses using a nonlinear fiber loop mirror, IEEE J. Quantum Electron. 35 (1999) 867–874.
[20] M. Attygalle, A. Nirmalathas, H.F. Liu, Novel technique for reduction of amplitude modulation of pulse trains generated by subharmonic synchronous mode-locked laser, IEEE Photon. Technol. Lett. 14 (2002) 543–545.
[21] M. Meissner, R. Rösch, B. Schmauss, G. Leuchs, 12 dB of noise reduction by a NOLM-based 2-R regenerator, IEEE Photon. Technol. Lett. 15 (2003) 1297–1299.
[22] A. Bogoni, P. Ghelfi, M. Scaffardi, L. Potì, All-optical regeneration and demultiplexing for 160-Gb/s transmission systems using a NOLM-based three-stage scheme, IEEE J. Sel. Top. Quantum Electron. 10 (2004) 192–196.
[23] N. Chi, L. Xu, K.S. Berg, T. Tokle, P. Jeppesen, All-optical wavelength conversion and multichannel 2R regeneration based on highly nonlinear dispersion-imbalanced loop mirror, IEEE Photon. Technol. Lett. 14 (2002) 1581–1583.
[24] Z. Huang, A. Gray, I. Khrushtchev, I. Bennion, 10 Gb/s transmission over 100 Mm of standard fiber using 2R regeneration in an optical loop mirror, IEEE Photon. Technol. Lett. 16 (2004) 2526–2528.
[25] S. Bigo, O. Leclerc, E. Desurvire, All-optical fiber signal processing and regeneration for soliton communications, IEEE J. Sel. Top. Quantum Electron. 3 (1997) 1208–1223.
[26] A.G. Striegler, B. Schmauss, Extinction ratio improvement by an advanced NOLM setup, IEEE Photon. Technol. Lett. 18 (2006) 1058–1060.

[27] S. Boscolo, J.H.B. Nijhof, S.K. Turitsyn, Autosoliton transmission in dispersion-managed systems guided by in-line nonlinear optical loop mirrors, Opt. Lett. 25 (2000) 1240–1242.
[28] S. Boscolo, S.K. Turitsyn, K.J. Blow, All-optical passive regeneration of 40 Gbit/s soliton data stream using dispersion management and in-line NOLMs, Electron. Lett. 37 (2001) 112–113.
[29] S. Boscolo, S.K. Turitsyn, K.J. Blow, Study of the operating regime for all-optical passive 2R regeneration of dispersion-managed RZ data at 40 Gb/s using in-line NOLMs, IEEE Photon. Technol. Lett. 14 (2002) 30–32.
[30] S. Boscolo, S.K. Turitsyn, K.J. Blow, Nonlinear loop mirror-based all-optical signal processing in fiber-optic communications, Opt. Fiber Technol. 14 (2008) 299–316.
[31] M.E. Fermann, F. Aberl, M. Hofer, H. Hochreiter, Nonlinear amplifying loop mirror, Opt. Lett. 15 (1990) 752–754.
[32] A.L. Steele, Pulse compression by an optical fibre loop mirror constructed from two different fibres, Electron. Lett. 29 (1993) 1872–1874.
[33] W.S. Wong, S. Namiki, M. Margalit, H.A. Haus, E.P. Ippen, Self-switching of optical pulses in dispersion-imbalanced nonlinear loop mirrors, Opt. Lett. 22 (1997) 1150–1152.
[34] E.A. Kuzin, N. Korneev, J.W. Haus, B. Ibarra-Escamilla, Theory of nonlinear loop mirrors with twisted low-birefringence fiber, J. Opt. Soc. Am. B 18 (2001) 919–925.
[35] T. Tanemura, K. Kikuchi, Circular-birefringence fiber for nonlinear optical signal processing, J. Lightwave Technol. 24 (2006) 4108–4119.
[36] O. Pottiez, E.A. Kuzin, B. Ibarra-Escamilla, F. Gutiérrez-Zainos, U. Ruiz-Corona, J.T. Camas-Anzueto, High-order amplitude regularization of an optical pulse train using a power-symmetric NOLM with adjustable contrast, IEEE Photon. Technol. Lett. 17 (2005) 154–156.
[37] O. Pottiez, B. Ibarra-Escamilla, E.A. Kuzin, High-quality amplitude jitter reduction and extinction enhancement using a power-symmetric NOLM and a polarizer, Opt. Express 15 (2007) 2564–2572.
[38] O. Pottiez, B. Ibarra-Escamilla, E.A. Kuzin, Demonstration of sharp switching from a power-symmetric NOLM and a polarizer, Opt. Commun. 271 (2007) 543–550.
[39] F. Doutre, D. Pagnoux, V. Couderc, A. Tonello, B. Vergne, A. Jalocha, Large temporal narrowing of subnanosecond pulses in a low-birefringence optical fiber, Opt. Lett. 33 (2008) 1789–1791.
[40] O. Pottiez, E.A. Kuzin, B. Ibarra-Escamilla, F. Mendez-Martinez, Theoretical investigation of the NOLM with highly twisted fibre and a $\lambda/4$ birefringence bias, Opt. Commun. 254 (2005) 152–167.
[41] C. Tsao, Optical Fiber Waveguide Analysis, Oxford University Press, New York, 1999.
[42] S.F. Feldman, D.A. Weinberger, H.G. Winful, Polarization instability in a twisted birefringent optical fiber, J. Opt. Soc. Am. B 10 (1993) 1191–1201.
[43] M. Horowitz, Y. Silberberg, Nonlinear filtering by use of intensity-dependent polarization rotation in birefringent fibers, Opt. Lett. 22 (1997) 1760–1762.
[44] R.H. Stolen, J.E. Bjorkholm, Parametric amplification and frequency conversion in optical fibers, IEEE J. Quantum Electron. 18 (1982) 1062–1072.

Olivier Pottiez was born in 1974 in Beloeil, Belgium. He received the Electrical Engineer and Ph.D. degrees from the Faculté Polytechnique de Mons (FPMs, Mons, Belgium) in 1997 and 2001, respectively. In 2003, he realised a postdoctoral stay at the Instituto Nacional de Astrofísica, Óptica y Electrónica (INAOE, Puebla, Mexico). He is currently a Researcher in the Fibre Optics Department of the Centro de Investigaciones en Óptica (CIO, León, Mexico). His present research interests include mode-locked fibre lasers for ultrashort pulse generation and fibre Sagnac interferometers for ultrafast photonics applications.

Baldemar Ibarra-Escamilla was born in Veracruz, Mexico, on April 9, 1969. He received the Bachelor degree in Electronics from the Benemerita Universidad Autonoma de Puebla, Mexico, in 1994. He received the M.S. and Ph.D. degrees in optics from the Instituto Nacional de Astrofísica, Optica y Electrónica (INAOE), Mexico, in 1996 and 1999, respectively. During 2000 he did a postdoctoral stay at the Electro-Optics Graduate Program, University of Dayton, USA. He is currently a Researcher of the Optics Department from the INAOE. His interests are in the field of optical fibre modelocked lasers, optical fibre amplifiers, tunable optical fibre lasers, and fibre-optic sensors.

Evgeny A. Kuzin was born in 1948 in St. Petersburg, Russia. He graduated from the University of St. Petersburg in 1976 and obtained the Ph.D. degree from the Phys-Technical Institute of Academy of Sciences of Russia in 1983. He was affiliated with the Phys-Technical Institute from 1976 to 1995, and since 1995 he is working at the National Institute of Astrophysics, Optics and Electronics, Puebla, Mexico.